Arch. Mech., **55**, 5–6, pp. 531–553, Warszawa 2003

High-accuracy discretization methods for solid mechanics

A. I. TOLSTYKH, M. V. LIPAVSKII, D. A. SHIROBOKOV

Computing Center of Russian Academy of Sciences
Vavilova str. 40, 119991 Moscow, Russia.
e-mail:tol@ccas.ru

NOVEL HIGH-ACCURACY computational techniques for solid mechanics problems are presented. They include fourth-order and arbitrary-order finite difference methods based on Pade-type differencing formulas and a meshless method which uses radial basis functions in a "finite difference" mode. Some results illustrating high performance of the suggested numerical methods are displayed.

1. Introduction

AT PRESENT, though the finite element method (FEM) is a universally accepted numerical tool in computational solid mechanics, the trend has been observed toward developing alternative techniques in the context of problem-oriented methodologies (for example, for solving problems with large deformations and moving discontinuities). Besides, one can see considerable interest in increasing the accuracy of numerical methods in a broad sense. The merits of high-accuracy methods can be manifested at least in two ways.

First, they may serve as high-resolution tools capable of describing properly fine details of solutions (for example, stress concentrations in small regions).

Second, they can provide engineering accuracy with relatively small numbers of degrees of freedom. As a result, operation counts and hence computational costs dramatically go down (mainly due to reducing by orders of magnitude the operation counts for both direct and iterative solvers of algebraic systems).

In the present paper, novel ideas are presented concerning applications of high-accuracy techniques to solid mechanics. They include:

(i) a finite difference method based on fourth-order compact differencing (CD) operators;

(ii) an arbitrary-order schemes for parallel calculations based on linear combinations of second-order CD operators (multioperators);

(iii) a meshless method which uses radial basis functions in a finite-difference mode.

The above methodologies are aimed at different areas of applications. While (i), (ii) show their peak performance in the case of relatively simple geometries

(for example, in the case of simply shaped plates and shells), using (iii) makes sense if the problem formulations include complicated forms of boundaries or/and an expected solution is that for which meshless methods are preferable.

Though (iii) differs in a significant way from (i) and (ii), both types of techniques, in contrast to the majority of the existing methods for solid mechanics, have in common the strategy of a direct discretization of governing equations rather than following their weak formulations. It makes them compatible when using them in the framework of the domain decomposition approach.

Below, the outlines of the methods followed by estimates of their performance in the case of testing solid mechanics problems are presented.

2. High accuracy schemes based on compact differencing

2.1. Fourth-order method

The well documented second-order difference schemes seem to be not popular in solid mechanics applications since they are approximately as accurate as the simplest FEM methods but they are considerably less flexible. However, recent advances in computational fluid dynamics have shown that high-order schemes can be highly competitive. Among such methods there are the so-called compact schemes which exploit Pade-type differencing formulas which can be viewed as rational functions of difference operators defined at compact stencils.

The simplest compact differencing formulas for the first and second derivatives are due to Collatz and Numerov. Supposing a uniform mesh with the mesh size h, the approximations to the derivatives at each grid point $x_j = jh$ look as

$$
\begin{aligned}
&D_x^{(1)} = (I + \Delta_2/6)^{-1}\,\Delta_0/(2h) = \partial/\partial x - (h^4/180)\,\partial^5/\partial x^5 + O(h^6),\\
&D_x^{(2)} = (I + \Delta_2/12)^{-1}\,\Delta_2/h^2 = \partial^2/\partial x^2 - (h^4/240)\,\partial^6/\partial x^6 + O(h^6),\\
&\Delta_0 f_j = f_{j+1} - f_{j-1}, \qquad \Delta_2 f_j = f_{j+1} - 2f_j + f_{j-1},
\end{aligned}
\tag{2.1}
$$

where I is the unity operator. The above formulas are not only fourth-order approximations, but they also have very small numerical coefficients in their truncation errors thus providing a very high accuracy.

Using Eqs. (2.1) for spatial x, y, z coordinates, one can easily discretize any form of solid mechanics equations. For example, for the biharmonic equation in the Cartesian coordinates describing the Kirchhoff plate, one has

$$
B_h w = D_x^{(2)} D_x^{(2)} w + D_y^{(2)} D_y^{(2)} w + 2 D_x^{(2)} D_y^{(2)} w = q,
$$

where q is a loading function. To calculate $B_h w$ where w is a known grid function, one needs only to perform several tridiagonal Gauss eliminations. The solutions

of the above equation can be obtained by using the standard iteration procedures. Since B_h is a self-adjoint positive operator in an appropriate Hilbert space, the convergence estimates for preconditioned iterations can be quite favorable. In the case of simply supported plates, it is advantageous to solve the biharmonic equation by sequentially solving two Poisson equations.

As an example of applications, consider a Kirchhoff plate occupying in the (x, y) plane the domain $\Omega: -l \leq x \leq l$, $0 \leq y \leq m$. The flexural rigidity of the plate $D(x, y)$ is supposed to be a sufficiently smooth function of its arguments, the only exception being its possible discontinuity at $x = 0$. It is supposed also that the plate may be strenghthened by a stiffener with the bending and torsional rigidities B and C respectively. Then the z-displacement w of the plate satisfies the biharmonic equation in both subdomains $-l \leq x \leq 0$, $0 \leq y \leq m$ and $0 \leq x \leq l$, $0 \leq y \leq m$ with proper boundary conditions at $\partial\Omega$. At $x=0$, the variational principle [1] gives the following "jump" conditions:

$$
\begin{aligned}
&\left\lceil w \right\rceil = 0, \quad \left\lceil w_{,x} \right\rceil = 0, \quad \left\lceil D(w_{,xx} + \nu w_{,yy}) \right\rceil = -(Cw_{,xy})_{,y}, \\
&\left\lceil \{D(w_{,xx} + \nu w_{,yy})\}_{,x} + 2\{D(1-\nu)w_{,xy}\}_{,y} \right\rceil = -(Bw_{,yy})_{,yy}
\end{aligned} \tag{2.2}
$$

where ν is the Poisson coefficient and for a function $f(x, y)$, $\left\lceil f \right\rceil$ means $f(+0, y) - f(-0, y)$. In the particular case $B=C=0$, $\lceil D \rceil = 0$, one has the interface conditions for the domain decomposition approach applied to plates with smoothly varying thickness.

Considering as an example the simply supported plate, we discretize the biharmonic equation using the above fourth-order compact differencing operators. To satisfy (2.2), a fifth-order formulas which relate $w_{,x}(-0, y)$ and $w_{,x}(+0, y)$ to w and $w_{,xx}$ at the "left" and "right" nodes respectively were constructed. Using them, a complete set of algebraic equations can be derived. In general, they can be solved by either direct or iterative solvers. The results presented below are obtained by alternately solving the "left" and "right" biharmonic equations.

The results of calculations with the standard-second order and the present fourth-order schemes for the square simply supported plates with a stiffener shown in Fig. 1 are presented in Table 1 for a sinusoidal load.

The bending and torsional rigidity of the stiffener were chosen as $B=2$ and $C=2$ respectively. The rigidity of the first plate $D=1$, (Fig. 1a) was assumed for both sides of the plate while the rigidity of the second plate was set to different values for each side of the plate ($D=1$, $x<0$, $D=2$, $x>0$, Fig. 1b).

In the Table 1, the L_2 norms of the solution errors δ and the corresponding mesh convergence order k are displayed for several $N \times N$ meshes, the reference "exact" solution being obtained using a very fine mesh.

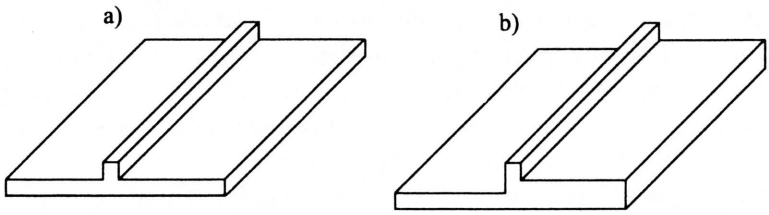

FIG. 1. Plates with stiffeners.

Table 1.

Plate	$D = 1$				$D = 1,\ x < 0;\quad D = 2,\ x > 0$			
Scheme	Second order		Fourth order		Second order		Fourth order	
$N \times N$	δ	k	δ	k	δ	k	δ	k
8×8	6.574e−3		3.532e−5		5.883e−3		4.941e−5	
16×16	1.582e−3	2.06	4.715e−6	2.91	1.395e−3	2.08	5.045e−6	3.29
32×32	3.870e−4	2.03	3.100e−7	3.93	3.386e−4	2.04	3.212e−7	3.97
64×64	9.566e−5	2.02	1.818e−8	4.09	8.339e−5	2.02	1.874e−8	4.10

As it may be seen from the Table 1, the present approach gives the solutions which are by several orders of magnitude more accurate than those obtained by the standard FD method (the latter is approximately as accurate as the FEM with linear elements). From the practical viewpoint, it means dramatic reduction of computational costs. For example, the fourth-order result for the 8×8 mesh is more accurate than the second-order one for 64×64 mesh. Note that the best algebraic solvers for two-dimensional cases give $O(N^2 \log N)$ operation counts.

2.2. Arbitrary-order discretizations

The standard FEM and FD methods (as well as the above described approach) are not able to enjoy in full measure the smoothness (or local smoothness) of exact solutions of many elasticity problems. Generally, they provide mesh-convergence orders which do not exceed the discretizations orders (the so-called "saturation" property). In contrast, accuracies of "saturation-free" methods depend on the numbers of existing exact solution derivatives (an interpolation with nodes chosen as zeroes of Chebyshev polynomials may serve as an example). On some occasions, the convergence can be exponential.

To increase the approximation the orders admitted by exact solutions smoothness, one usually tries to increase the values of some parameters defining the discretizations (for example, polynomial orders of local interpolants). In many cases,

it may complicate the resulting formulas and create some problems when implementing the constructed algorithms. An alternative way was suggested in [2] in the context of the parallel computational fluid dynamics. Its essence is using linear combinations ("multioperators") of special types of basis operators having relatively simple structures to provide theoretically arbitrary-order schemes. Recently [3], the idea was extended to the case of centered discretizations appropriate for solid mechanics equations.

To describe the extension, we return to operators (2.1) and consider without any loss of generality the x-derivatives only. Changing the coefficients $1/6$ and $1/12$ by a parameter c, we obtain one-parametric families $D_x^{(1)}(c)$ and $D_x^{(2)}(c)$ approximating the first and second derivatives with the second (rather than the fourth) order. Fixing now M distinct values of c, $(c = c_1, c_2, \ldots c_M)$, one can define multioperators for the x-derivatives [3]

$$D_M^{(1)} = \sum_{i=1}^{M} \gamma_i D_x^{(1)}(c_i), \qquad D_M^{(2)} = \sum_{i=1}^{M} \bar{\gamma}_i D_x^{(2)}(c_i),$$

where γ_i and $\bar{\gamma}_i$ satisfy the following linear systems:

$$\sum_{j=1}^{M} \gamma_j = 1, \quad \sum_{j=1}^{M} c_j^k \gamma_j = r_k, \quad k = 1, 2, \ldots M-1, \tag{2.3}$$

$$\sum_{j=1}^{M} \bar{\gamma}_j = 1, \quad \sum_{j=1}^{M} c_j^k \bar{\gamma}_j = \bar{r}_k, \quad k = 1, 2, \ldots M-1, \tag{2.4}$$

where r_k and $\bar{r}_k$ are known constants obtainable from the Taylor expansion series for the actions of $D_x^{(1)}(c_i)$ and $D_x^{(2)}(c_i)$ on sufficiently smooth functions projected into the space of grid functions. For example, in the case of $M = 3$, one has $(r_1, r_2) = (1/24, 3/640)$ and $(\bar{r}_1, \bar{r}_2) = (1/6, 1/30)$.

The above systems with the Vandermonde matrices are known to be always uniquely solvable. Moreover, their solutions can be easily obtained in analytical forms.

One can prove the following

THEOREM 1. *Let $u \in C^{2M}$ and $\gamma_1, \gamma_2, \ldots, \gamma_M$, $\bar{\gamma}_1, \bar{\gamma}_2, \ldots, \bar{\gamma}_M$ denote the solutions of (2.3), (2.4) for $c_i \neq c_j$, $i \neq j$, $i, j = 1, 2, \ldots, M$. Then*

$$D_M^{(1)} = \partial/\partial x + O(h^{2M}), \qquad D_M^{(2)} = \partial^2/\partial x^2 + O(h^{2M}).$$

To relax the ill-conditioning property of systems with the Vandermonde matrix when $M \to \infty$, we suppose that c_i are zeroes of the Chebyshev polynomials

for an interval $[c_{\min}, c_{\max}]$. Further limitations on the choice of c_i in the case of second derivatives follow from the requirement that multioperators must be negative definite, thus providing good convergence properties of relevant iterative procedures. For $M=3$, the sufficient conditions can be obtained in an analytical form [3].

Using multioperators for each coordinate, one can discretize any solid mechanics equation. The resulting schemes are especially advantageous when using parallel machines (at least, M processors are needed). In that case, the $2M$-th order admitted by the degree of solutions smoothness is realized by simultaneous and synchronous calculations of actions of basis operators. So the computational costs, when calculating actions of multioperators on a known grid function, turn out to be the same as those in the case of a single basis operator with a simple architecture.

To illustrate possible peak performance of the multioperators method, we consider the following BVP for the Poisson equation

$$\Delta u = -2\pi^2 \sin \pi x \sin \pi y,$$

$$x, y \in \Omega = [0,1] \times [0,1], \quad u|_{\partial\Omega} = 0.$$

Its exact solution is $\sin \pi x \sin \pi y$. The same exact solution can be obtained for the biharmonic equation describing bending of a square plate

$$\Delta\Delta u = 4\pi^4 \sin \pi x \sin \pi y, \quad x, y \in \Omega \tag{2.5}$$

with boundary conditions $u|_{\partial\Omega}=0$; $\partial^2 u/\partial x^2 = 0$ for $x=0, 1$; $\partial^2 u/\partial y^2 = 0$ for $y=0, 1$.

Sixth-order operators $D_M^{(2)}$ corresponding to the x and y coordinates ($M=3$) with proper restrictions imposed on c_1, c_2, c_3 were used to approximate the Laplace operator. In the case of problem (2.5), the biharmonic operator was considered as the square of the Laplace one.

The results for both problems for several meshes are shown in Table 2 ($N \times N$ stands for the number of grid points while k is the estimated mesh-convergence order).

As it may be seen from Table 2, the numerical solution accuracy is very high even if only 4 grid points are placed in each spatial directions. Again, the most important output of using the methodology is the possibility of obtaining an engineering accuracy with a very small number of degrees of freedom since it means computational costs savings up to many orders of magnitude. However, it should be emphasized that the technique exploits the solution smoothness. So its efficiency depends on the quality of meshes in the case of complicated geometries. In that case, one may suggest to use it in the framework of a domain

decomposition by constructing subdomains with "good" and "bad" boundaries. The latter category can be treated by using other methods. In particular, the multioperators method can be combined with the meshless radial basis function technique described in the next section.

Table 2.

Problem	Poisson eq.		Biharmonic eq.	
$N \times N$	δ	k	δ	k
4×4	2.31e−6		4.62e−6	
6×6	3.28e−7	4.81	6.57e−7	4.81
12×12	6.23e−9	5.72	1.24e−8	5.73
24×24	1.01e−10	5.95	2.01e−10	5.95

3. Using meshless interpolants in a finite differencing mode

Recently, considerable attention has been paid in computational solid mechanics to the so-called meshless methods allowing to discretize PDEs using scattered nodes. They have some attractive features. In particular, they do not require structured or unstructured grids thus automatically obviating the difficulties of constructing high quality meshes needed, for example, in the case of the above described technique. Meshless methods are known to greatly simplify the solution procedures in the cases of large deformations, changing geometries etc. Among the first meshless methods, there are generalized finite difference [4] and smooth particle hydrodynamics [5] methods. The majority of existing meshless methods exploit the least squares principle to construct meshless approximations. In these approaches, the approximated functions and their approximations, in general, do not coincide at the nodes. They are used mainly in the framework of the Galerkin method (their extensive review can be found for example in [6]).

Another approach is using radial basis functions (RBF), that is the functions of arguments which are distances between current point and nodes. In contrast to the least squares approximations, RBF interpolants satisfy the interpolation conditions stating that they are equal to the interpolated functions at nodes. It was found that the RBF interpolation procedure has the potential for being very accurate providing in some instances exponential convergence. The overview and the relevant references concerning RBF can be found, for example, in [7].

Unlike the least-squares types methods, RBF applications to PDEs are based mainly on the collocation and boundary elements strategies [8–10]. The merits of the collocation RBF techniques are simplicity of boundary conditions formulations and absence of numerical integration procedures typical for some

meshless Galerkin-type methods. However, serious problems may arise due to the ill-conditioning property of the resulting linear systems. To circumvent the difficulty, some remedies were proposed. They concern locally supported RBF [11–13]; preconditioning [14] and domain decomposition [15].

We consider here another way of using the RBF suggested in [16]. The idea is to define for each node a local set of neighbour nodes ("stencils", following finite differencing terminology), to construct for the set an RBF interpolant and the resulting approximations to derivatives at the node. The approximation formulas can be then used when discretizing the PDE of interest.

The procedure is completely analogous to the finite difference one. It differs from the latter in

(1) using arbitrary spaced nodes instead of grid points,
(2) using RBF instead of polynomials when constructing numerical differentiation formulas.

Comparing with the collocation approach, the governing equations are approximated at each node rather than satisfied at the node. Using local RBF supports greatly relaxes the ill-conditioning limitation. Assuming on good RBF approximation properties, one may expect reasonable high accuracy.

In what follows, the technique is presented in more details.

3.1. RBF approximations to derivatives and RBF schemes

Suppose one has a set $X = \{\mathbf{x}_1, \mathbf{x}_2, \ldots, \mathbf{x}_M\} \subset \Omega$ of nodes in a computational domain Ω. Let $X_j = (\mathbf{x}_1^{(j)}, \mathbf{x}_2^{(j)}, \ldots, \mathbf{x}_{N_j}^{(j)})$, $X_j \subset X$, $\mathbf{x}_j \in X_j$ be a "cloud" of nodes surrounding each node $\mathbf{x}_j$. The node will be referred to as a center of the cloud. Following the finite difference terminology, we shall however use the notion "stencil" instead of cloud.

Suppose further that $u(\mathbf{x})$, $\mathbf{x} \in \Omega$ is a sufficiently smooth function. Denoting $u(\mathbf{x}_i) = u_i$, let us introduce "internal" numbering for a subset X_j: if $\mathbf{x}_i = \mathbf{x}_k^{(j)}$ then $u_i = u_k^{(j)}$ where k is some number from $(1, 2, \ldots, N_j)$.

We construct for each X_j an interpolant

$$s^{(j)}(\mathbf{x}) = \sum_{k=1}^{N_j} c_k^{(j)} \phi(||\mathbf{x} - \mathbf{x}_k^{(j)}||),$$

where $||\cdot||$ is the Euclidean norm, $b_{ki}^{(j)}$ are the entries of the matrix which is inverse of the coefficients matrix $A^{(j)} = \{a_{ik}^j\} = \{\phi(||\mathbf{x}_i - \mathbf{x}_k^{(j)}||\}$ arising from the interpolation conditions $s^{(j)}(\mathbf{x}_k^{(j)}) = u_k^{(j)}$, $k = 1, 2, \ldots, N_j$.

For any linear differential operator D one can construct then the approximate formula $[Du]_j \approx c_k^{(j)}[D\phi(||\mathbf{x} - \mathbf{x}_k^{(j)}||)]_j$ where the notation $[Df]_j = Df|_{\mathbf{x}=\mathbf{x}_j}$

is used. Substituting the expression for $c_k^{(j)}$, one may write finally

$$[Du]_j \approx \sum_{i=1}^{N_j} (c_D)_i^{(j)} u_i^{(j)},$$

$$(3.1) \qquad (c_D)_i^{(j)} = \sum_{k=1}^{N_j} b_{ki}^{(j)} [D\phi(||\mathbf{x} - \mathbf{x}_k^{(j)}||)]_j, \quad j = 1, 2, \ldots, M.$$

The coefficients $(c_D)_i^{(j)}$ depend only on D and the coordinates of the nodes belonging to the j-th stencil. They do not vary during the solution processes (if nodes are not moving) and can be calculated during preprocessing.

In the following, we shall suppose that D is an operator of derivatives with respect to Cartesian coordinates. Then (3.1) may be viewed as usual numerical differentiation formulas written for stencils X_j. Such formulas are used for discretizations of PDEs when each internal node considered as a center leads to algebraic systems with sparse matrices typical for a conventional finite difference method. It is worth noting that it is possible to use "oriented" stencils for skew-symmetric operators, thus introducing an upwinding used in fluid dynamics applications.

Differencing formulas (3.1) can be readily extended to the case when derivatives are specified at data points (for example, near the boundaries where the Neumann boundary conditions are used). In that case we suppose that values $f_i = f(\mathbf{x}_i^{(j)})$ are specified at some nodes of the j-th stencil $\mathbf{x}_1^{(j)}, \mathbf{x}_2^{(j)}, \ldots, \mathbf{x}_p^{(j)}$ while functionals $Df|_{\mathbf{x}=\mathbf{x}_k^{(j)}}$ are given at $\bar{\mathbf{x}}_1^{(j)}, \bar{\mathbf{x}}_2^{(j)}, \ldots, \bar{\mathbf{x}}_q^{(j)}$ where D is a linear operator. It is assumed that $\mathbf{x}_i^{(j)}$ and $\bar{\mathbf{x}}_k^{(j)}$ possibly coincide for certain i and k.

The corresponding RBF interpolant has the form

$$s^{(j)}(\mathbf{x}) = \sum_{k=1}^{p} a_k \phi(||\mathbf{x} - \mathbf{x}_k^{(j)}||) + \sum_{k=1}^{q} b_k D^{(x)} \phi(||\mathbf{x} - \bar{\mathbf{x}}_k^{(j)}||),$$

$$p,\ q < N_j,$$

where (x) indicates the action of D on ϕ as a function of x. Requiring that

$$s^{(j)}(\mathbf{x}_k^{(j)}) = f(\mathbf{x}_k^{(j)}),$$

$$Ds^{(j)}|_{\mathbf{x}=\bar{\mathbf{x}}_k^{(j)}} = Df|_{\mathbf{x}=\bar{\mathbf{x}}_k^{(j)}},$$

one obtains the following linear system:

$$
\begin{pmatrix}
\phi_{11}...\phi_{1p} & D\phi_{11}...D\phi_{1q} \\
\vdots & \vdots \\
\phi_{p1}...\phi_{pp} & D\phi_{p1}...D\phi_{pq} \\
D\phi_{11}...D\phi_{1p} & D^2\phi_{11}...D^2\phi_{1q} \\
\vdots & \vdots \\
D\phi_{q1}...D\phi_{qp} & D^2\phi_{q1}...D^2\phi_{qq}
\end{pmatrix}
\begin{pmatrix}
a_1 \\ \vdots \\ a_p \\ b_1 \\ \vdots \\ b_q
\end{pmatrix}
=
\begin{pmatrix}
f_1 \\ \vdots \\ f_p \\ Df_1 \\ \vdots \\ Df_q
\end{pmatrix}, \tag{3.2}
$$

$\phi_{ij} = \phi(||\mathbf{x}_i - \mathbf{x}_j||)$, $D\phi_{ij} = D\phi(||\mathbf{x} - \mathbf{x}_j||)|_{\mathbf{x}=\mathbf{x}_i}$, $D^2\phi_{ij} = D^2\phi(||\mathbf{x} - \mathbf{x}_j||)|_{\mathbf{x}=\mathbf{x}_i}$.

Assuming that matrix (3. 2) does not degenerate (this is the case for certain types of ϕ), one can solve the system for coefficients a_k, b_k. Applying operator D to $s(\mathbf{x})$ at a node $\mathbf{x}_j$, one obtains the following generalization of (3. 1):

$$
D_\alpha \approx \sum_{k=1}^{p} C_k^{(\alpha)} f_k + \sum_{k=1}^{q} B_k^{(\alpha)} Df_k,
$$

where the coefficients $C_k^{(\alpha)}$ and $B_k^{(\alpha)}$ depend on the coordinates of the nodes forming the j-th stencil while D_α is supposed to be the operator of the αth-order derivative in one direction or another.

It is of interest to estimate the actual accuracy of (3. 1) in the cases when D is the operator of the first or second partial derivatives and N_j are reasonably small numbers. Unfortunately, in contrast to the usual FD formulas, the Taylor expansion series are not very efficient here. It is due to degeneration of the coefficient matrix in the limit of vanishing distances between neighbour points.

There are some estimates of the h-convergence in the case of cardinal interpolation [25], when nodes x_j are generated by the Cartesian grid with $N_j = \infty$.

A natural but not a general way to estimate the approximation errors for relatively small N_j is their direct calculation for certain classes of functions. Of course, it gives only some impression concerning the RBF performance in a finite difference mode. The results of the calculations for Hardy multiquadrics (MQ)

$$
\phi(r) = (r^2 + C)^{1/2}, \qquad r^2 = x^2 + y^2, \tag{3.3}
$$

with $C = 1$ are presented in [16]. Figure 2 shows L_2 – norms of errors in the case of the first and second derivatives of $f(x) = \exp(2(x + y))$ when using the stencils indicated herein.

It can be seen from Fig. 2 that the norms can be well presented by the power laws h^p where h is the distance between nodes while $p = 2, 4, 6$ for stencils $1, 2, 3$. For a fixed $h = h_*$, enlarging the stencils increases the accuracy of the derivatives discretization. However, one should not expect that this will continue when the

number of nodes $N_j = K$ in the stencils increases without bound. When $K \to \infty$, the accuracy of the interpolation which provides differencing formulas is expected to tend to that of the cardinal interpolation [26], for $h = h_*$.

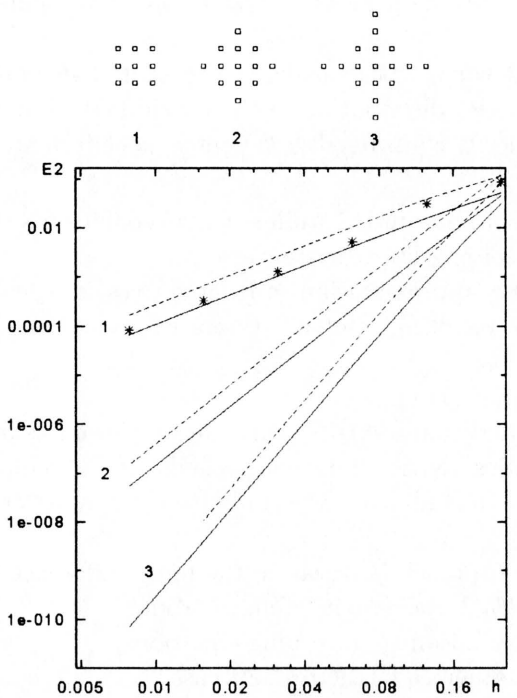

FIG. 2. Mean-root-square errors vs. mesh size and the corresponding RBF stencils. Solid and dashed lines correspond to first and second derivatives respectively.

In the figure, the result obtained with the second-order-accurate centered finite difference formula for the first derivative are also shown (marked by asterisks). They are close to those for the stencil 1.

Discretization at each node of a given PDE can be proceeded in a standard finite difference manner by changing derivatives with their approximations. Assembling then the resulting algebraic equations and using the boundary conditions (which, if needed, can be discretized as well), one obtains a global system for unknown nodal variables.

In the linear case, its matrix is a sparse one and the system can be solved using direct or iterative methods. In the numerical experiments described below the direct nested dissection method [27] was used. It should be noted that condition numbers for "global" systems were found to be quite acceptable. However, though the present technique suggests $N_j \ll N$, ill-conditioning of a system like (3.2) can not be ruled out if N_j is too large or distances between the nodes are

too small. In the calculations, the situation has been encountered only in the h-convergence studies when very small values of h, the characteristic distances between nodes, were used. In those cases, quadro precision arithmetic was exploited. The preconditioning ideas of [14] seems to be quite attractive to deal with such cases.

Summing up, to solve a PDE using the present RBF approach, one should:

(i) Specify the nodes distribution in the considered computational domain;

(ii) For each node x_j considered as a center, specify a stencil with N_j nodes surrounding x_j;

(iii) For each stencil, obtain the "differencing" coefficients (for example $(c_D)_i^{(j)}$ in (3.1)) by solving linear systems;

(iv) Substitute the approximations to derivatives at each node in the PDE and form the resulting "global" system by assembling together the nodal approximations;

(v) Solve the global system.

It should be noted that steps (i)–(iii) can be viewed as a preprocessing procedure once the nodes distributions and stencils are not supposed to be changed during calculations. In nonlinear cases, only steps (iv) and (v) have to be included in iterations.

Since the RBF approach is based on the finite difference principle, the theorem stating that $O(h^k)$ convergence follows from

(i) $O(h^k)$ approximation to governing equations,

(ii) stability of a schemes in the present case.

Unfortunately, it is difficult to prove both properties in a general case of arbitrarily spaced nodes and arbitrary stencils. However, the potential for satisfying (i) and (ii) was discussed in [16] where it was shown that the RBF approximation to the Laplace operator using stencil 1 from Fig. 2 is a negative definite one (the Hilbert space of double-periodic nodal functions with the inner product $(u, v) = h^2 \sum_{i,j} u_{ij} v_{ij}$ where u_{ij} and v_{ij} are defined at grid points $x_i = ih, y_j = jh$ of the Cartesian grid was assumed). As a result, in that case (as well as in the cases of other stencils shown in Fig. 2), very fast convergence was observed when using the simplest iterative procedure for inverting the corresponding L_h operators.

In the calculations described below, h-convergence was always seen at least for the considered ranges of h and all the considered stencils.

Though general RBF methodology is really a meshless one and a random nodes distribution can be used, the most accurate numerical solutions can be expected only if a "proper" distribution is specified depending on the problem to be solved. Moreover, the strategy of choosing stencils in the present approach, as in the finite difference methods, plays an important role.

Since the calculations presented below are aimed mainly at comparisons with other methods, either triangulated or Cartesian meshes were used as nodes distributions. As to step (ii), different strategies were used when specifying stencils.

In the following, the MQ radial basis functions will be considered only. We set $C = 1$ in (3.3) when carrying out the majority of the calculations described below since we are not aware of the existence of a theory giving an optimal choice of C. Of course, judging from the results presented in [17, 18], the solution accuracy is expected to be lower than that for a more successful choice of C.

3.2. Numerical examples

EXAMPLE 1. KIRCHHOFF PLATES

We consider below two cases of the Kirchhoff plates for which exact solutions are available. Their bending is described by the biharmonic equation. In the particular case of simply supported edges, a solution procedure can be reduced to successive solutions of two Poisson equations.

The first case is a square plate problem described by (2.5). The calculations were carried out using seven-points "simple" (or RBF-1) and nineteen-points (or RBF-2) "enlarged" stencils (Fig. 3), the fourth-order technique from Sec. 2 and the FEM method with linear elements. The L_2 norms of errors are displayed in Fig. 4. As it is seen, the "simple" stencils and FEM show second-order mesh convergence while the RBF with "enlarged" stencil and CD method are fourth-order accurate. At the same time, the RBF solutions are more accurate than their counterparts of the same order.

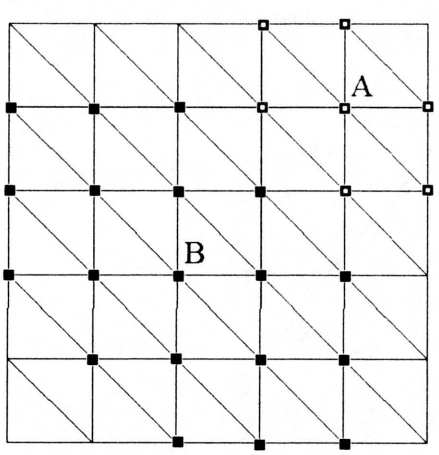

FIG. 3. A triangulated mesh in a square domain. The "simple" stencil for the node A and the "enlarged" stencil for the node B are shown by white and black markers respectively.

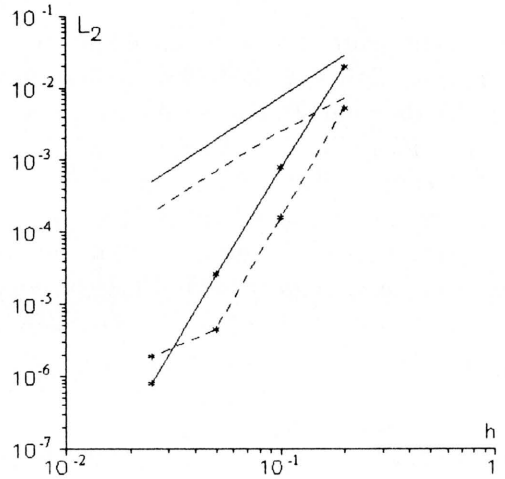

Fig. 4. Mean-root-square errors vs. mesh size for the biharmonic equation in a square domain. Dashed lines without markers and with markers correspond to the RBF "simple" and "enlarged" stencils respectively. Solid lines without markers and with markers correspond to FEM and compact scheme of fourth-order respectively.

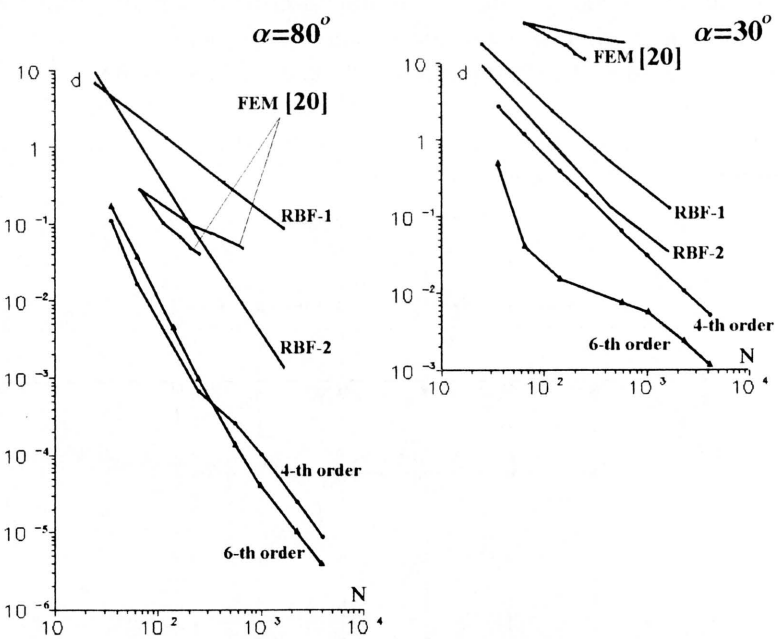

FIG. 5. Relative center displacement error for rhombic plate vs. number of nodes (on percentage basis).

As the next testing example, we consider bending of a simply supported rhombic plate subjected to a uniform load. In that case, there is a singularity of the exact solution which has an adverse effect on the accuracy of numerical methods. The problem is investigated in [20] in the context of performance of several finite element methods. Then the most accurate solutions obtained with 21 degrees of freedom elements using both uniform and non-uniform meshes are compared with the present RBF and CD results.

Figure 5 displays the relative center displacement errors (on a percentage basis) vs. the number of nodes in the computational domain for two values of the rhomb angle. The exact solution considered as a reference one was obtained using the technique described in [21], while the most accurate are the solutions obtained with the fourth-order CD and sixth-order CD-based multioperators schemes. However, the mesh-convergence orders in all cases are not so high as in the previous example. Moreover, the performance of the fourth and sixth-order methods is approximately identical though the latter is slightly more accurate.

EXAMPLE 2. TORSION OF PRISMATIC BARS

According to the elasticity theory, solutions of the bar torsion problems can be obtained by solving the Dirichlet problem for the Poisson equation

$$\triangle\phi = -2,\ \mathbf{x} \in \boldsymbol{\Omega}, \qquad \phi|_{\partial\boldsymbol{\Omega}} = \mathbf{0},$$

where Ω is a bar cross-section domain. The corresponding stress components can then be expressed in terms of x- and y-derivatives of ϕ. In the case of cross-sections with boundaries which contain "incoming" angles which rounded vertices, it is of interest to predict accurately the stress concentrations near the rounded corners where high gradients are possible (it is known that stresses become singular when the corresponding curvature radii tend to zero).

We consider the geometry of a bar cross-section shown in Fig. 6 which was investigated in [22] using very accurate semi-analytic method. The cross-section is characterized by the radius r of the rounded corner and the "shelf" length A, the "shelf" thickness being assumed to be unity. The asymptotics in the case $r \to 0$ was investigated in [19, 22]. To describe properly the stresses near point C for small r, high-accuracy methods are needed.

The RBF calculations were carried out using triangulated meshes (one of them is shown in Fig. 6). The meshes are defined by numbers M and N of nodes uniformly distributed along the boundary PQ and the boundary RS, respectively. Thus the condensation of nodes near C can be achieved by increasing M.

To compare the solution $K = \text{grad}\,\phi$ in C with the results of [22], the ϕ derivatives were approximated using the third-order four-points formula. The calculations were carried out for three meshes $M=11$, $N=20$; $M=21$, $N=40$ and $M=41$, $N=80$ showed that the difference between the results corresponding to the second and the third meshes could be estimated as 0.2%.

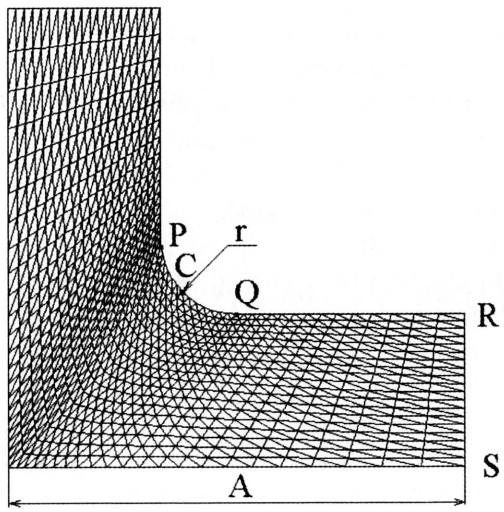

FIG. 6. L-shaped domain with rounded incoming corner.

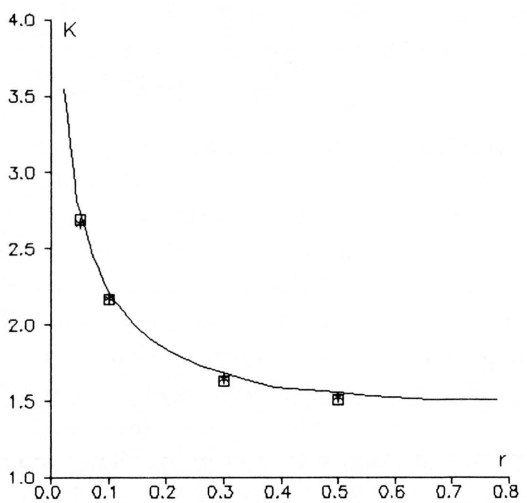

FIG. 7. The stress concentration parameter K vs. radius of the rounding.

Figure 7 displays the K values obtained for $A=3$ and $r=0.5, 0.3, 0.1, 0.05$ using the "simple" stencil defined on the coarsest mesh (markers as squares) and finest mesh (markers as stars), the difference between the values being about 1.2% (an exception is the case $r = 0.05$). The curve depicted in Fig. 7 corresponds to the "almost exact" solution for $A = \infty$. Since the influence of A is quite insignificant in the domain $A > 3$ (the results for $A=3$ and $A=4$ differs by 0.2%), the agreement is rather good.

Another comparison with the solution from [22] is shown in Fig. 8. In the figure, the ratio K/A for the fixed value $r/A = 0.1$ is presented as a function of $1/A$. Again one may see that the present results (markers) agree closely with those from [22] (solid line).

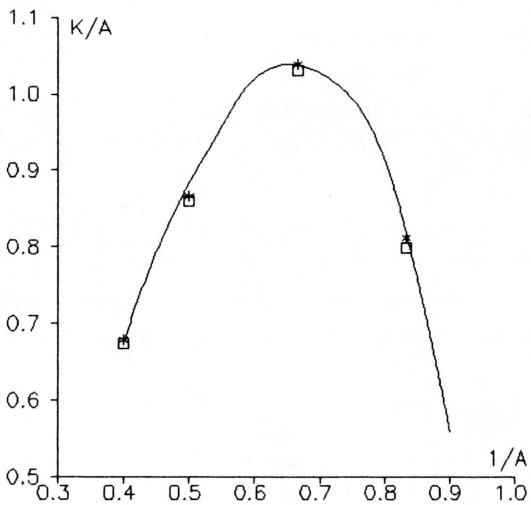

FIG. 8. The parameter K/A vs. $1/A$. The solid line and markers correspond to results from [22] and the present results respectively.

EXAMPLE 3. CANTILEVER BEAM

Consider now the application of the described approach to one of the 2D elasto-statics problems, namely to the cantilever beam problem which is popular when verifying meshless methods (see for example [6], [23]). The governing equations this time are

$$\sigma_{xx,x} + \sigma_{xy,y} = 0, \qquad \sigma_{xy,x} + \sigma_{yy,y} = 0,$$

where, assuming the plane-stress case, $\sigma_{xx} = (u_{,x} + \nu v_{,y})E/(1-\nu^2)$, $\sigma_{xy} = (u_{,y}+v_{,x})E/(2(1-\nu^2))$, $\sigma_{yy} = (v_{,y}+\nu u_{,x})E/(1-\nu^2)$ and u, v are displacements in the x- and y-directions and E is the elasticity modulus. We set $E = 1000$, $\nu = 0.3$ as in [23]. As boundary conditions, the displacements defined by the exact solutions were used. The exact solutions for the cantilever beam problem can be found in [24].

The equations were approximated at nodal points which were distributed in the same manner as those in the above cited publications.

Though an optimal choice of stencils is beyond the scope of the present paper, different strategies of their forming were tried. One of them was as follows. For each center $\mathbf{x}_j$, the stencil was defined as a set of nodes which fall on a domain

S_j : $\mathbf{x}_j \in S_j$ with a prescribed shape of its boundary and a prescribed characteristic length R (the latter was, for example, a circle radius, the edge of a rectangle etc.) or a characteristic area.

In the present case, grid points of regular $M \times N$ meshes were used as nodes. The beam length and width are L=12 and D=2 respectively.

Figure 9 presents L_{uv} solution errors as functions of the mesh size h_x in the x-direction for several stencils with nodes falling on circles, squares, ellipses with the axis length ratio 2 : 1 and rectangles with the aspect ratio 2 : 1, the area of the supports being $20h_x^2$ and $50h_x^2$. The L_{uv} errors are defined as

$$L_{uv} = \left(\sum_i (u_i - u_{ei})^2 + (v_i - v_{ei})^2 / \sum_i u_{ei}^2 + v_{ei}^2 \right)^{1/2},$$

where u_{ei} and v_{ei} are the exact values at a i-th node and the summation is carried out over the nodes of the computational domain.

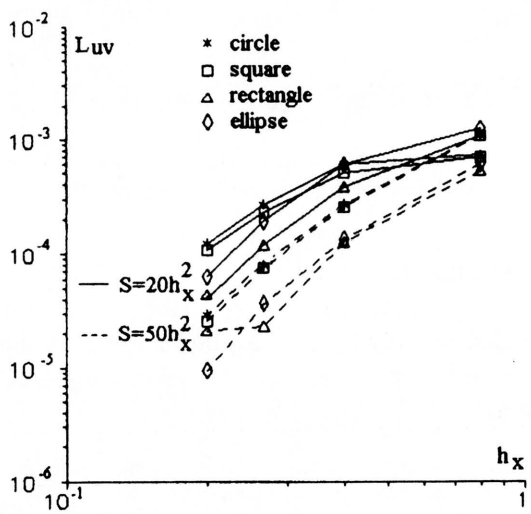

FIG. 9. The cantilever beam problem: relative errors of displacements vs. mesh size h_x for several stencils and areas of supports.

As seen in Fig. 9, the influence of the supports type is not very significant in the present case, the best choice being ellipses. As may be expected, enlarging stencils improves the accuracy and the convergence rate. However, it does not necessary mean that the improvement will continue by including more and more nodes in stencils.

Once the numerical solutions for displacements are obtained, the corresponding stress calculations may be viewed as a postprocessing procedure. A rich vari-

ety of RBF approximations to derivatives using different stencils can be used. In the present particular case, finite difference formulas were found to be effective.

Figure 10 presents the relative errors in the stresses σ_{xx} and σ_{xy} as defined in [23] for the calculations with the elliptical supports.

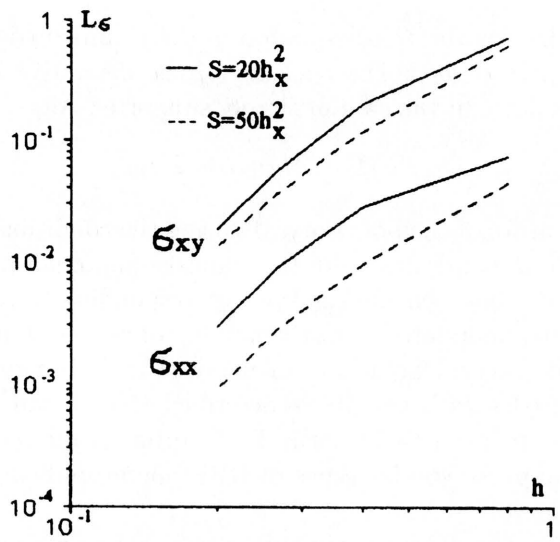

FIG. 10. The cantilever beam problem: relative errors of stresses vs. mesh size h_x for two areas of ellipsis.

EXAMPLE 4. NONLINEAR SHELL DEFORMATIONS

As another example of the present RBF technique application, we consider a nonlinear shell problem described by the Kármán–Föppl equations [28].

Based on the Kirchhoff assumptions, the equations for a plate having thickness h=const read

$$u_{1,xx} + w_{,x}w_{,xx} + 0.5(1+\nu)(u_{2,xy} + w_{,y}w_{,xy}) + 0.5(1-\nu)(u_{1,yy} + w_{,x}w_{,yy}) = 0,$$

$$u_{2,yy} + w_{,y}w_{,yy} + 0.5(1+\nu)(u_{1,xy} + w_{,x}w_{,xy}) + 0.5(1-\nu)(u_{2,xx} + w_{,y}w_{,xx}) = 0,$$

$$D\triangle\triangle w = q + (Eh/(1-\nu^2))\{[u_{1,x} + \nu u_{2,y} + 0.5w_{,x}^2 + 0.5\nu w_{,y}^2]w_{,xx}$$
$$+ [u_{2,y} + \nu u_{1,x} + 0.5w_{,y}^2 + 0.5\nu w_{,x}^2]w_{,yy} + (1-\nu)[u_{1,y} + u_{2,x} + w_{,x}w_{,y}]w_{,xy}\}.$$

In the above equations, u_1, u_2, w are the displacements of a plate middle surface corresponding to the Cartesian coordinates x, y, z respectively. It is supposed that the coordinates origin is at the surface, the axis z being normal to it.

In the following, simply supported edges or clamped edges will be assumed. In both cases, the boundary conditions for the first two equations and the condition for the third equation are

$$u_1|_\Gamma = u_2|_\Gamma = w|_\Gamma = 0.$$

The second condition for the third equation in the clamped edges case has the form $\partial w/\partial n = 0$ where $\partial/\partial n$ is the operator of the derivative in the direction normal to the boundary. In the case of simply supported edges, it reads

$$\triangle w + (1-\nu)k\partial w/\partial n = 0,$$

where k is the curvature of the boundary. By using the condition, one can avoid, as indicated in [29], a manifestation of the Babuska-Saponjan paradox which is an essential difference between the solutions corresponding to round plates and plates with polygonal boundaries with the number of vertices tending to infinity.

In the calculations, grid points of an unstructured triangulated grid were assumed as RBF nodes with the above described RBF-1 and RBF-2 stencils. To discretize the fourth derivatives, the RBF formulas for second derivatives were sequentially applied, special types of RBF operators being used near the boundaries.

As a test problem, consider bending of a round plate with simply supported or clamped edges under uniform loading. Due to the central symmetry, the highly accurate solution can be obtained by solving ordinary differential equations. The solution is used as a reference one. For the triangulated mesh, the number of nodes N along the radial directions were chosen to be $N = 6, 11, 21$.

Table 3. Simply supported edges.

	"simple" stencils			"enlarged" stencils		
Q	$N=6$	$N=11$	$N=21$	$N=6$	$N=11$	$N=21$
L	0.63957	0.67898	0.69090	0.70145	0.69596	0.69532
0.5	0.28053	0.29235	0.29592	0.29971	0.29761	0.29728
1	0.46222	0.47478	0.47869	0.48400	0.48091	0.48030
2	0.68697	0.69773	0.70141	0.70817	0.70407	0.70311
4	0.95080	0.95867	0.96192	0.97005	0.96499	0.96368
6	1.12568	1.13163	1.13459	1.14343	1.13788	1.13638

In Tables 3 and 4, the center displacements of the plate $W = w_{\text{center}}/h$ are presented for various values of the dimensionless load $Q = q(R/h)^4/E$ and the above mentioned values of N, h and R being the plate thickness and the plate radius, respectively. The Poisson coefficient is assumed to be 0.3. For comparison,

the reference solution (column "ref") and the results for the linear case with $Q = 1$ (string "L" in Tables 3) are also included in the tables. It should be noted that the exact solution for the latter case is $W = .695625$.

Table 4. Clamped edges.

	"simple" stencils			"enlarged" stencils			
Q	$N = 6$	$N = 11$	$N = 21$	$N = 6$	$N = 11$	$N = 21$	ref
1	0.15725	0.16459	0.16704	0.16536	0.16744	0.16789	0.16785
2	0.30479	0.31693	0.32094	0.31906	0.32173	0.32234	0.32250
4	0.55499	0.56900	0.57538	0.57537	0.57501	0.57524	0.57625
6	0.75126	0.76252	0.76619	0.77366	0.76824	0.76773	0.76956

As it can be seen, the difference between the RBF and reference solution does not exceed 0.5% for $N = 21$ in the case of the RBF-1 stencil and 0.2% for $N = 11$ in the case of the RBF-2 stencil.

As an example of a more complicated geometry, Fig. 11 presents the dependence "W vs. Q" where W and Q are the above defined variables. The plate boundary is given by $r = R(1 + \cos(6\phi)/5)$ in the polar coordinates (r, ϕ), the nodes distribution being shown in the figure. One can see considerable difference of the results obtained in the frameworks of linear and nonlinear theory.

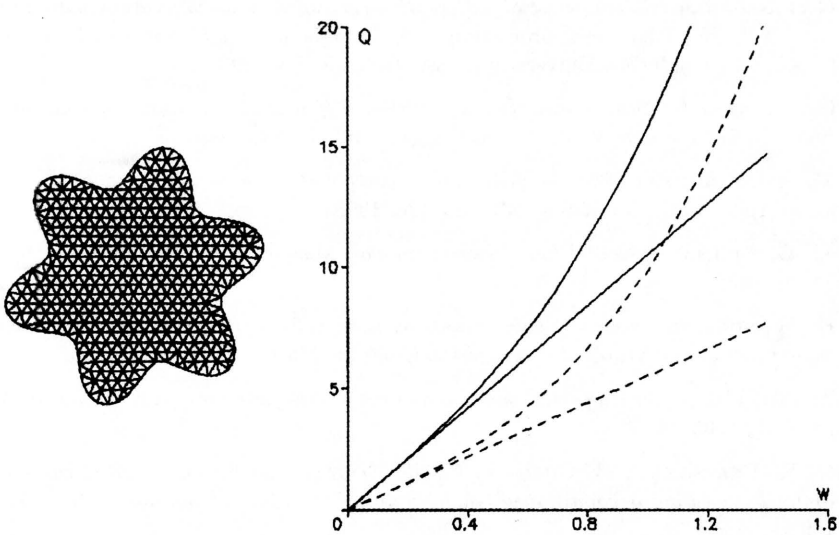

FIG. 11. A mesh for a plate with complicated geometry. Q vs W. Solid and dashed lines correspond to simply supported and clamped edge respectively.

Acknowledgment

This work was supported by INTAS, project N1150 and Russian Fund of basic researches, grant 02-01-00436.

References

1. A. A. SAMARSKII, V. B. ANDREEV, *Finite difference methods for elliptic equations* (in Russian), Izd. Nauka, Moscow 1976.
2. A. I. TOLSTYKH, *Multioperator high-order compact upwind methods for CFD parallel calculations,* [in:] Parallel Computational Fluid Dynamics, D. R. Emerson, A. Ecer, J. Periaux and N. Satofuka [Eds.], 383–390, Elsevier, Amsterdam 1998.
3. A. I. TOLSTYKH, *On prescribed order integro-interpolation schemes,* J. Comput. Math and Math. Phys. (transl. from Russian), to appear in 2002.
4. T. LIZKA, J. ORKITZ, *The finite difference method at arbitrary irregular grids and its application in applied mechanics,* Comput. Struct., **11**, 83–95, 1980.
5. J. J. MONAGHAN, *Why particle methods work,* SIAM J. Sci. Stat. Comput., **3**, 422–433, 1982.
6. T. BELYTCHKO, Y. KRONGAUS, D. ORGAN, M. FLEMING, P. KRYSL, *Meshless methods: An overview and recent developments,* Comp. Meth. Appl. Eng., **139**, 3–47, 1996.
7. E. J. KANSA, R. E. CARLSON, *Radial basis function: a class of grid-free scatterel data approximations,* Comput. Fluid Dynamics J., **3**, 479–496, 1995.
8. G. FASSHAUER, *Solving partial differential equations with collocation with radial basis functions,* [in:] Chamonix proceedings, A. LeMehaute, C. Robut and L. L. Shunaker [Eds.], 1–8, Vanderbilt University Press, Nashville TN 1996.
9. C. FRANKE, R. SCHABACK, *Solving partial differential equations by collocation using radial basis functions,* Appl. Math. Comput., **93**, 73–82, 1998.
10. M. A. ZERROUKAT, *Fast boundary element algorithm for time-dependent potential problems,* Appl. Math. Modelling, **22**, 183–196, 1998.
11. M. D. BUHMANN, *Radial functions on compact support.* Proc. Edinburg Math. Soc., **41**, 33–46, 1998.
12. H. WENDLAND, *Piecewise polynomial, positive definite and compactly supported radial basis functions of minimal degree,* Adv. Comput. Math., **4**, 386–396, 1995.
13. Z. WU, *Compactly supported positive definite radial functions,* Adv. Comput. Math., **4**, 283–292, 1995.
14. R. K. BEATSON, J. B. CHERRIE, C. T. MONAL, *Fast fitting of radial basis functions. Methods based on preconditioned GMRES iteration,* Adv. in Comput. Math., **11**, 253–270, 1999.
15. S. M. WONG, Y. C. HON, T. S. LI, S. L. CHUG, E. J. KANSA, *Multizone decomposition of time dependent problems using the multiquadric scheme,* Comput. Math. Appl., **37**, 23–45, 1999.

16. A. I. TOLSTYKH, *On using RBF-based differencing formulas for unstructured and mixed structured-unstructured grid calculations,* [in:] Proceedings of 16th IMACS World Congress, Lausanne 2000.

17. E. J. KANSA, *Multyquadrics – a scattered data approximation scheme with applications to fluid dynamics – II: Solutions to parabolic, hyperbolic and elliptic partial differential equations*, Comput. Math. Appl., **19**, 147–161, 1990.

18. E. J. KANSA, Y. C. HON, *Circumventing the ill-conditioning problem with multiquadric radial basis functions: Applications to elliptic partial differential equations*, Comput. Math. Appl. **39**, 123–137, 2000.

19. G. I. MARCHUK, V. I. AGOSHKOV, *Introduction to projective-difference methods* (in Russian), Izd. Nauka, Moscow 1981.

20. I. BABUSKA, T. SCAPOLLA, *Benchmark computation and performance evaluation for a rhombic plate bending problem*, Int. J. Num. Meth. Eng., **28**, 155–179, 1989.

21. L. S. D. MORLEY *Skew plates and Structures. International Series of Monographs in Aeronautics*, Macmillan, New York 1963.

22. V. I. VLASOV, D. B. VOLKOV, *Multypole method for solving Poisson equation in domains with rounded angles*, Zh. Vychisl. Mat. Mat. Fiz., **35**, 6, 867–872, 1995.

23. X. ZHANG, K. Z. SONG, M. W. LU, X. LIU, *Meshless methods based on collocation with radial basis functions,* Comput. Mech., **26**, 333–343, 2000.

24. S. P. TIMOSHENKO, S. N. GOODIER, *Theory of elastisity*, McGraw-Hill, New York 1970.

25. W. R. MADYCH, S. A. NELSON, *Error bounds for multiquadric interpolation,* [in:] Approximation theory VI, C. K. CHUI, L. L. SHUMAKER, J. W. WARDS [Eds.], Academic Press, New York 1989.

26. M. D. BUHMANN, *Multivariate cardinal interpolation with radial-basis functions,* Constructive approximations, **6**, 225–255, 1990.

27. A. GEORGE, J. W-H LIU, *Computer Solution of Large Sparse Positive Definite Systems,* Prentice-Hall, New Jercey 1981.

28. E. I. GRIGOLUK, V. I. MAMAI, *Nonlinear deformation of thin-wall construction* [in Russian], Izd. Nauka Fizmatlit, Moscow 1997.

29. V. G. MAZJA, S. A. NAZAROV, *Paradoxes of the solutions of boundary value problem on the smooth domain approximated by polygons,* Izv. Akad. Nauk USSR, Ser. Mat., **50**, 1156–1177, 1986.

Received March 21, 2003; revised version July 1, 2003.